ELSEVIER

Chemical Geology 239 (2007) 64–82

CHEMICAL GEOLOGY
INCLUDING
ISOTOPE GEOSCIENCE

www.elsevier.com/locate/chemgeo

Compositions of high Fe–Ti eclogites from the Sulu UHP metamorphic terrane, China: HFSE decoupling and protolith characteristics

Yung-Hsin Liu [a], Huai-Jen Yang [a,*], Yen-Hong Shau [b], Fancong Meng [c], Jianxin Zhang [c], Jingsui Yang [c], Zhiqin Xu [c], Shu-Cheng Yu [a]

[a] *Earth Dynamic System Research Center and Department of Earth Sciences, National Cheng-Kung University, Tainan, 70101, Taiwan*
[b] *Department of Marine Biotechnology and Resources, National Sun Yat-Sen University, Kaohsiung, 80424, Taiwan*
[c] *Institute of Geology, Chinese Academy of Geological Sciences, Beijing 100037, China*

Received 12 October 2006; received in revised form 30 November 2006; accepted 17 December 2006

Editor: R.L. Rudnick

Abstract

Eclogite protoliths provide clues for understanding paleomagmatism and tectonic architecture. A subgroup of eclogites from Maobei in the Sulu metamorphic terrane in eastern China are characterized by (1) low SiO_2 contents of 38.2–42.8%, (2) high FeO_{total} abundances of 16.7–20.9%, (3) high TiO_2 concentrations of 3–4%, and (4) decoupling between high field strength elements (HFSE), specifically, Ti enrichment accompanied by relative depletions in Nb–Ta–Zr–Hf. These features are also characteristic of eclogites cored by the Chinese Continental Scientific Drilling (CCSD) project at the depth range of 530–600 m (subunit 8). Except for the relatively low SiO_2 concentrations, major element concentrations of these high Fe–Ti eclogites are comparable to those of basalts and gabbros. The low SiO_2 reflects the combined effect of fluid infiltration and garnet enrichment by metamorphic segregation. In contrast, there is no evidence for rutile segregation, and the high TiO_2 contents are protolith characteristics. The major and trace element abundances as well as the decoupling between Ti and other HFSEs in these high Fe–Ti eclogites are interpreted as characteristics of gabbroic cumulates crystallized from melts with compositions similar to that of the CCSD eclogites cored at depth ranges of 318–380 and 420–470 m (subunits 4 and 6, respectively). The mineral proportions of such cumulates are ~41% plagioclase, ~39% clinopyroxene, ~8% olivine and ~12% Fe–Ti oxides, consistent with crystallization at 2–8 kbar. The basaltic melts in equilibrium with the gabbroic protoliths of the high Fe–Ti eclogites must be depleted in Nb, Ta, Zr and Hf. These are the characteristics of arc lavas and crustally contaminated continental basalts. An arc origin for these protoliths is consistent with the existence of arc belts on the margins of the Yangtze Block during protolith formation. However, this does not preclude contemporary plume magmatism within the interior of the Yangtze block.

Keywords: Sulu; Eclogites; HFSE; CCSD; Protolith; Metamorphic differentiation

1. Introduction

The Dabie–Sulu metamorphic terrane in east-central China formed during collision between the southern

* Corresponding author. Tel.: +886 6 275 7575 #65429.
E-mail address: hjyang@mail.ncku.edu.tw (H.-J. Yang).

0009-2541/$ - see front matter © 2006 Elsevier B.V. All rights reserved.
doi:10.1016/j.chemgeo.2006.12.005

Yangtze and northern Sino–Korean cratons. Volumetrically minor eclogites in this metamorphic terrane have Nd isotope ratios with continental affinities, which together with the occurrence of coesite have led to a general model of subducting continental lithosphere to ultrahigh-pressure (UHP) conditions (e.g., Jahn, 1998). Geochronological studies of these eclogites indicate protolith ages of 600–850 Ma and metamorphic ages of 220 Ma (e.g., Li et al., 1993, 2000; Ames et al., 1996). Because the protoliths of the Dabie–Sulu eclogites are contemporary with the Neoproterozoic magmatism in the Yangtze Block, they add constraints to the debated tectonic architecture of the Rodinia supercontinent. For example, Li et al. (2003) proposed that the Neoproterozoic magmatism was produced by a "superplume" event that separated the Yangtze Block from the Rodinia supercontinent. In contrast, Zhou et al. (2002) used the occurrence of 760–860 Ma arc-related mafic intrusions in the margins of the Yangtze Block to argue that the Yangtze Block was isolated from the Rodinia supercontinent by ancient oceans during Neoproterozoic time.

In addition to the tectonic implications inferred from their protoliths, eclogites are also proposed to be components in the sources of mid-ocean ridge basalts (MORB; e.g., Hirschmann and Stopler, 1996), ocean island basalts (OIB; e.g., Huang and Frey, 2005) and large igneous provinces (LIP; e.g., Leitch and Davies, 2001). Eclogites may also be geochemical reservoirs complementary to continental crust and depleted mantle (Rudnick et al., 2000). Clearly, eclogite compositions are important for understanding the chemical evolution of the earth. However, constraints on the eclogite compositions are mainly derived from eclogite xenoliths and orogenic eclogites having oceanic affinities. The compositions of orogenic eclogites having continental affinities, such as the Dabie–Sulu eclogites, are not as well characterized.

The compositional range of Dabie–Sulu eclogites was defined by Jahn (1998), who used major and trace element compositions of 32 samples from 10 localities in the Dabie terrane and 18 samples from 6 localities in the Sulu terrane to show that the Dabie–Sulu eclogites are mainly basaltic in composition but some formed as cumulates. Their major oxide abundances vary significantly with SiO_2, MgO, Al_2O_3, CaO and Na_2O contents in the ranges of 40–60%, 3–14%, 11–21%, 6–15%, and 0.6–4.6%, respectively, reflecting the combined effects of igneous, metamorphic, and in some cases, metasomatic processes (Jahn, 1998; Jahn et al., 2003a, 2005). The petrogenetic relationships between eclogites from different localities have not been established. Unusual features in the data of Jahn (1998) are the distinctively high TiO_2 contents of 11.4% in one sample and 3.81–4.77% in three samples from the Dabie terrane. High TiO_2 eclogites are also exposed at Maobei in southern Sulu terrane and were cored by the Chinese Continental Scientific Drilling (CCSD) project (Zhang et al., 2004). The high TiO_2 contents are accompanied by high total iron of >18.5% (as ferric iron). Understanding the unusually high Ti and Fe abundances in these eclogites and their petrogenetic and tectonic implications requires trace element and isotopic constraints. In this study, we analyzed five high Fe–Ti eclogites and one high-Ti garnetite from Maobei for major and trace element abundances as well as $^{87}Sr/^{86}Sr$ and $^{143}Nd/^{144}Nd$ ratios. Integrating our results and the published CCSD data, we aim to understand (1) the roles of protolith compositions, metamorphic differentiation, and metasomatism in controlling compositional variations of the high Fe–Ti eclogites, (2) the processes causing high Ti abundances and decoupling of Ti from other high field strength elements, and (3) the petrogenetic link between the high Fe–Ti eclogites and other eclogites. With these petrogenetic constraints, we infer the pre-subduction tectonic architecture and suggest that subduction of high Fe–Ti eclogites into mantle may be an important process.

2. Geological background

The Sulu metamorphic terrane, bounded by the Wulian–Qingdao–Yantai fault (WQYF) on the northwest and the Jiashan–Xianshui fault (JXF) on the south, is offset ~530 km to the north of the Dabie terrane by the western Tanlu fault (Fig. 1). It is divided into the northern UHP and the southern high-pressure (HP) belts (Zhang et al., 1995) (Fig. 1). The HP belt consists of quartz–mica schists, marbles and rare blueschists. The UHP belt consists of eclogites, granitic gneisses, amphibolites, schists, and marbles, which were subjected to in-situ metamorphism at 700–890 °C and >28 kbar, then overprinted by granulite–amphibolite-facies retrogression. Eclogites and serpentinized peridotites occur as layers and blocks in gneisses and schists or as "boudins" and nodules in marbles (e.g., Zhang et al., 1995). These metamorphic rocks are overlain by Jurassic sedimentary and Cretaceous volcanoclastic successions intruded by post-orogenic Mesozoic granites. Near Maobei, a large N–S trending eclogite–ultramafic complex (3000 m × 250–300 m) within gneissic rocks forms an NNE-trending overturned fold with an SE dipping axial plane (Su et al., 2005). On the eastern limb of the fold, we collected samples from an eclogite layer exposed on the wall of a pit (34°25′ N,

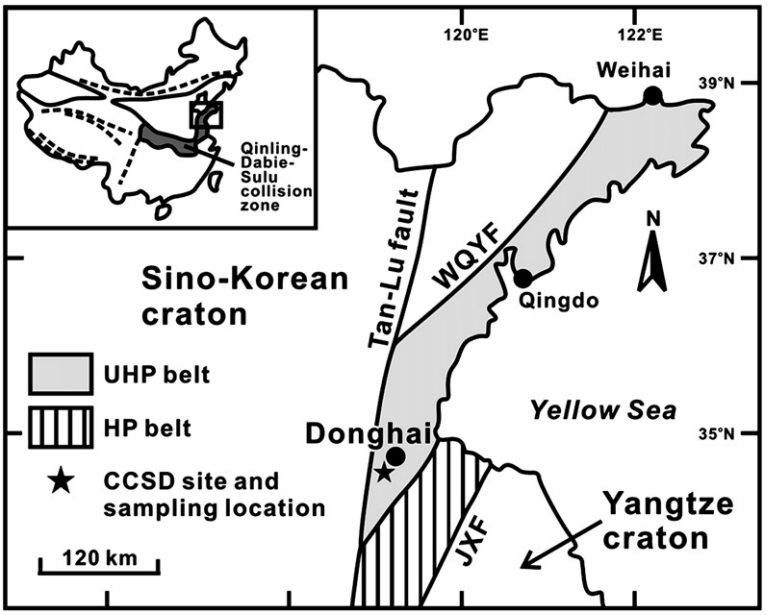

Fig. 1. Simplified map enlarged from the rectangle in the insert map of China showing the location of Donghai county in the Sulu UHP metamorphic terrane, which is bounded by the Wulian–Qingdo–Yantai fault (WQYF), Jiashan–Xianshui fault (JXF) and Tan–Lu fault. See text for the descriptions of the northern UHP and southern HP belts. The star indicates the Chinese Continental Scientific Drilling site (34°25′ N, 118°40′ E). The studied samples were collected from Maobei, 300 m northwest from the Chinese Continental Scientific Drilling site. The inset map of China shows the locations of major suture zones (dashed curves) and the Qinling–Dabie–Sulu metamorphic terrane.

118°40′ E) located 300 m northwest of the drilling site of the CCSD project (Fig. 1). The pit is 5 m deep with an area of ~100 m^2. The eclogite layer is 3–4 m thick exposed on the lower portion of the wall and is overlain by a layer of unconsolidated soil.

3. Petrographic descriptions

Collected specimens are approximately 20 × 15 × 7 cm^3. Garnet is abundant, 53–60 vol.%, followed by 30–42 vol.% omphacite (Table 1). There is no obvious garnet–omphacite banding (Fig. 2a). Garnet is anhedral and some grains contain rutile (Fig. 2b) and omphacite inclusions but are free of quartz, mica, and epidote inclusions that are commonly observed in garnet from many other eclogite suites (Jahn et al., 2005). These garnet grains also lack coronas of amphibole, quartz, plagioclase, and secondary clinopyroxene, which typically form during retrogression (Zhang et al., 1995). Omphacite grains are mostly subhedral and free of inclusions (Fig. 2c). They occur as individual grains and aggregates of 3–6 grains. All the analyzed samples contain accessory rutile (1–4 vol.%) and amphibole (1–5 vol.%). Veins with width <2 mm, occur in samples MB002, 0717 and 0720. They consist of hornblende, ilmenite, epidote, albite, quartz, apatite and titanite (Fig. 2c). Omphacite grains near the veins are often recrystallized to plagioclase and amphibole forming a symplectite texture. While sharing these common features, the analyzed eclogites vary in grain size and mineral proportions (Table 1).

Samples MB001 and D56 contain coarse-grained garnet and omphacite (1.5–2 mm) accompanied by fine-grained (<1 mm) interstitial rutile (Fig. 2b). Approximate 2 vol.% amphibole occurs along grain boundaries of garnet, omphacite, and rutile. Sample MB002 has

Table 1
Mineral assemblages and proportions (%) in the high Fe–Ti eclogites and garnetite

Rock type sample	High Fe–Ti eclogite					Garnetite
	MB001	D56	MB002	0720	0717	0722
Garnet	52.7	57.0	54.0	60.5	59.3	80.5
Omphacite	42.1	37.0	40.5	30.0	29.2	–
Rutile	3.4	4.0	3.7	2.7	<1	<1
Amphibole	1.6	2.0	<1	5.4	5.5	<1
Fe–Ti oxide	<1	–	–	1.0	5.0	17.4
Epidote	–	–	–	<1	<1	<1
Apatite	–	–	<1	–	–	<1
Plagioclase	<1	–	–	–	–	–
Titanite	–	–	–	<1	<1	–
Garnet /omphacite	1.25	1.54	1.33	2.01	2.03	–

Mineral proportions were determined by >3000 point counts on the vein-free portions of each sample.

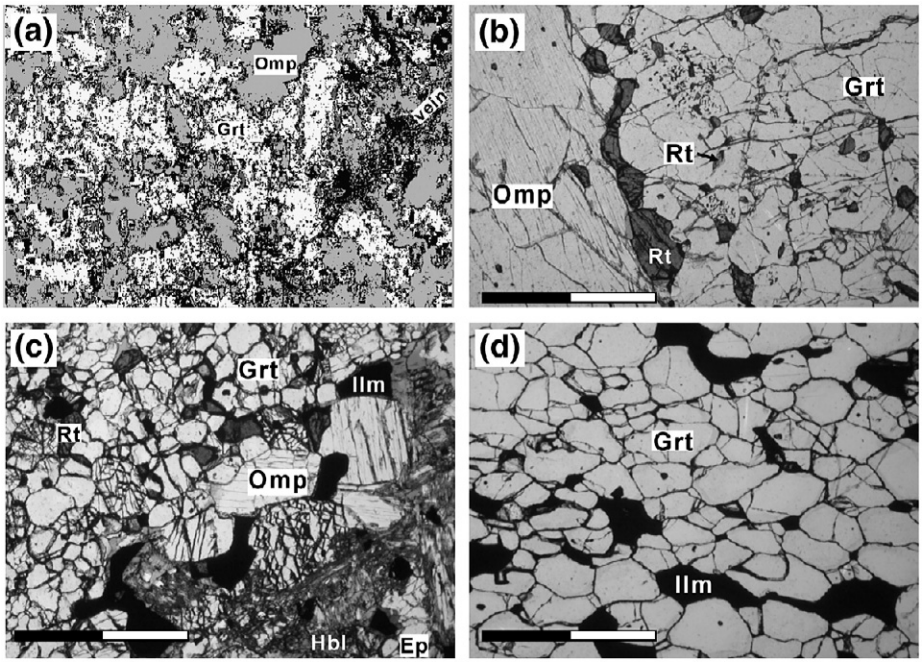

Fig. 2. Panel (a) is an image processed picture for the thin section (4×3 cm^2) of sample MB002 showing the absence of obvious metamorphic banding of garnet (Grt; white) and omphacite (Omp; dark grey). A vein (black) infiltrates the eclogite at the lower right portion of this view. Panels (b), (c), and (d) are photomicrographs taken in plane-polarized light showing textures of high Fe–Ti eclogites and garnetite. (b) Rutile in sample MB001 occurs as inclusions or as interstitial grains between garnet and omphacite. (c) A vein (lower right of this view) in sample MB002 consists of hornblende (Hbl), epidote (Ep) and ilmenite (Ilm). (d) Elongated garnet and Fe–Ti oxides are dominant phases in the garnetite. Scale bars in panels b–d are 1 mm.

relatively fine-grained (~0.5 mm) and nearly inclusion-free garnet; omphacite grains are rounded or elongated with sizes varying from <0.1 to 1.5 mm. The vein-free aliquots of samples MB001, MB002, and D56 have garnet/omphacite ratios ranging from 1.3 to 1.5 (Table 1). Samples 0717 and 0720 are fine-grained like sample MB002 but their vein-free aliquots have higher garnet/omphacite ratios of >2 with more amphibole (~5 vol. %) that occurs as up to 0.5 mm grains (Table 1). Sample 0717 also contains more Fe–Ti oxides (5 vol.%) with <1 vol.% rutile (Table 1).

Sample 0722 contains mainly garnet and Fe–Ti oxides (Fig. 2d), with accessory rutile, amphibole, apatite, and epidote (Table 1); it is subsequently referred to as "garnetite". In this sample, equigranular zoned garnet show core to rim increases in almandine. Fe–Ti oxides grains comprise Fe-rich and Ti-rich domains and some rutile grains are rimmed by Fe–Ti oxides. Amphibole and epidote occur in veins or as interstitial grains around garnet and Fe–Ti oxides.

4. Analytical methods

Major compositions of garnet and omphacite were determined with a JEOL JXA-8900R 4-spectrometer electron microprobe at the Institute of Earth Sciences, Academia Sinica using 15 kV accelerating voltage and 10 nA beam current. Beam size was approximately 1 μm for garnet and 2 μm for other silicate phases. The data were reduced using ZAF matrix corrections (Goldstein et al., 1981).

For bulk analyses, >100 g of each sample was powdered to reduce the possible heterogeneity caused by metamorphic differentiation, even though mineral banding is not obvious at hand specimen and thin section scales. It is not certain whether the chemical constituents of vein minerals were exotic or derived from eclogite forming minerals, although the former is generally inferred. To evaluate the compositional heterogeneities caused by the veins, the vein-free and vein-containing aliquots of three samples were analyzed. Major oxide abundances were measured from fused glasses using the X-ray fluorescence spectrometer (XRF) at the National Taiwan University (NTU) and University of Massachusetts (U. Mass) in Amherst following the methods of Chung et al. (2003) and Rhodes and Vollinger (2004), respectively. Results from these two laboratories for the same samples are within 5% (Table 3).

For trace element analysis, 100 mg of sample powder was fluxed in a HF–HNO_3 mixture at 190 °C in a high-pressure bomb for at least 24 h, then followed by a sequential process of heating to dryness, dissolution in HCl, conversion to nitric form, and finally a factor of 1000 dilution in a ~2% nitric solution. Four of the six samples were duplicated by the same procedures except for addition of ~0.1% HF to final solutions containing ~2% HNO_3 in order to minimize element adsorption on container walls (Münker, 1998). The final solutions were analyzed with an inductively coupled plasma mass spectrometer (ICP-MS; Agilent 7500S) at NTU for the abundances of 14 rare earth elements (REEs), 5 high field strength elements (HFSEs; refer to Ti, Nb, Ta, Zr and Hf), and 9 other trace elements (Table 3). The US Geological Survey (USGS) standards PCC-1, BCR-2, BIR-1 and AGV-1 were used to establish calibration curves. Standard BHVO-1 was run as an external standard to evaluate accuracy and the results are within 5% of the recommended values (Eggins et al., 1997). Duplicates of BHVO-1 indicate that the precisions were within 10% for all analyzed elements, mostly ≤3% (Table 3). Results from duplicates of HNO_3-based and HNO_3–HF-based solutions agree within 5%, except for low abundance elements (Rb, Nb, Ta, and some LREE), which can differ by ~15% (Table 3). Abundances of Ti, Sr, Zr and Y were also determined by the XRF at U. Mass in Amherst following the method of Rhodes and Vollinger (2004) and the results agree with the ICP-MS data within 10% (Table 3). The Ti data obtained by ICP-MS and XRF are within 4%, except 7–8% for two samples, indicating complete dissolution of Fe–Ti oxides in the ICP solutions.

For Sr and Nd isotopic analyses, 70 mg of sample powder was decomposed in an HF–HNO_3 mixture, taken to dryness followed by dissolution in 2 ml HCl (2 N) and loaded onto a column containing AG50W-X8, 100–200 mesh resin to extract Sr and REEs. The REE portion was passed through the column containing Eichrom Ln resin to extract Nd. About 250 ng of Sr and Nd were loaded onto a thermal ionization mass spectrometer (TIMS; Finnigan MAT262) at the Department of Earth Sciences of National Cheng-Kung University for isotopic analyses. Procedural blanks for Sr and Nd were <200 pg. Mass fractionation was corrected using $^{146}Nd/^{144}Nd = 0.7219$ and $^{86}Sr/^{88}Sr = 0.1194$. During the course of this study, the mean $^{87}Sr/^{86}Sr$ ratios were 0.710242±10 ($n=15$) for NBS 987 and 0.705036±40 ($n=7$) for BCR-1, whereas the mean $^{143}Nd/^{144}Nd$ ratios for LaJolla and BCR-2 were 0.511835±12 ($n=12$) and 0.512608±24 ($n=6$), respectively.

5. Results

5.1. Mineral compositions

Although garnet and clinopyroxene in the analyzed eclogites are unzoned, there are compositional differences between grains in each sample and between samples. Garnet compositions vary in the range of $Alm_{44.0–60.0}Pyp_{15.6–20.2}Grs_{24.0–36.5}Sps_{0.5–0.8}$ (Table 2). The garnet grains in the high Fe–Ti eclogites have higher grossular and lower almandine contents than those in the garnetite (Table 2, Fig. 3a). Most clinopyroxene grains contain 20–28% jadeite component falling in the compositional range of omphacite (Table 2, Fig. 3b). Few grains near the veins have lower jadeite contents of 13–18% (Fig. 3b).

5.2. Whole-rock major and trace element compositions

The analyzed eclogites have 6.03–7.01% MgO, 12.6–17.4% Al_2O_3, 11.2–12.5% CaO, and 1.60–2.45% Na_2O (Table 3), all within the ranges of basalts and gabbros (Fig. 4). However, compared to basalts and gabbros with similar MgO contents, these eclogites have slightly lower SiO_2 (38.2 to 42.8%) but higher FeO_{total} (total iron as ferrous iron is 16.7–20.9%) and TiO_2 (~3.5%) (Fig. 4). The vein-free aliquots of samples 0717 and 0720 have higher Al_2O_3 contents than their corresponding vein-containing aliquots (17% vs 12.6% for 0717; 17.1% vs 13.2% for 0720; Table 3). Sample 0720 has a slightly higher SiO_2 content in the vein-containing aliquot (Table 3). Except for these discrepancies, there are no significant differences between other major oxide contents of the vein-free and corresponding vein-containing aliquots of each sample (Table 3). However, vein-containing aliquots of samples generally have slightly higher incompatible element contents and Sr/Nd and Ba/Th ratios than their corresponding vein-free aliquots (Table 3). When element abundances are normalized to the primitive mantle values, all the analyzed samples show enrichment in Ti but depletions in other HFSEs (Fig. 5). This is a peculiar feature, since HFSEs generally behave coherently during magmatic processes. In general, middle-REEs (MREEs) and light-REEs (LREEs) together form concaved-upward REE patterns (Fig. 6).

The analyzed eclogites are compositionally similar to the eclogites cored by CCSD at the depth range of 530–600 m (subunit 8). Zhang et al. (2004) described these CCSD eclogites as “high Fe–Ti eclogites”, a term that we use for our samples. The CCSD project also

Table 2
Compositions of garnet and omphacite in the high Fe–Ti eclogites and garnetite from Maobei, Sulu UHP metamorphic terrane

Rock type	High Fe–Ti eclogite			Garnetite	High Fe–Ti eclogite		
Sample	MB001	MB002	D56	0722	MB001	MB002	D56
Mineral	Garnet				Omphacite		
SiO_2	38.4	39.3	38.8	38.4	55.1	55.7	54.5
TiO_2	0.17	0.08	0.08	0.01	–	0.13	0.05
Al_2O_3	20.7	21.1	21.2	21.9	5.74	6.41	5.88
FeO	24.7	23.2	25.0	27.2	9.27	8.26	8.43
MnO	0.29	0.33	0.35	0.27	–	–	–
MgO	5.09	5.49	4.11	4.14	9.66	9.47	9.90
CaO	10.6	11.8	11.2	8.82	15.6	14.5	16.0
Na_2O	–	–	–	0.02	4.94	6.01	5.03
Total	99.9	101.3	100.7	100.7	100.2	100.3	99.7
Cations/12 oxygens					Cations/6 oxygens		
Si	3.001	3.003	3.009	2.991	1.997	1.997	1.978
Ti	0.010	0.004	0.005	0.001	–	0.004	0.001
Al	1.910	1.895	1.937	2.007	0.245	0.271	0.251
Fe^{3+}	–	–	–	–	0.107	0.145	0.144
Fe^{2+}	1.612	1.482	1.621	1.770	0.174	0.102	0.112
Mn	0.019	0.022	0.023	0.018	–	–	–
Mg	0.593	0.625	0.475	0.480	0.522	0.506	0.536
Ca	0.885	0.966	0.927	0.736	0.606	0.555	0.623
Na	–	–	–	0.004	0.347	0.418	0.354
Total	8.031	7.997	7.997	8.007	3.998	3.998	3.999
Component percentages (%)							
Alm	51.8	47.9	53.2	58.9	–	–	–
Pyp	19.1	20.2	15.6	16.0	–	–	–
Grs	28.5	31.2	30.4	24.5	–	–	–
Sps	0.61	0.70	0.80	0.60	–	–	–
Ac	–	–	–	–	10.7	14.5	14.4
Jd	–	–	–	–	24.0	27.3	21.0
Aug	–	–	–	–	65.3	58.2	64.6

sampled eclogites containing >3% TiO_2 at the depths of 318–380 and 420–470 m (subunits 4 and 6). However, these eclogites are distinct from the "high Fe–Ti eclogites" in having lower total iron and higher trace element abundances with the absence of HFSE decoupling; they were referred to as "high-Ti eclogites"

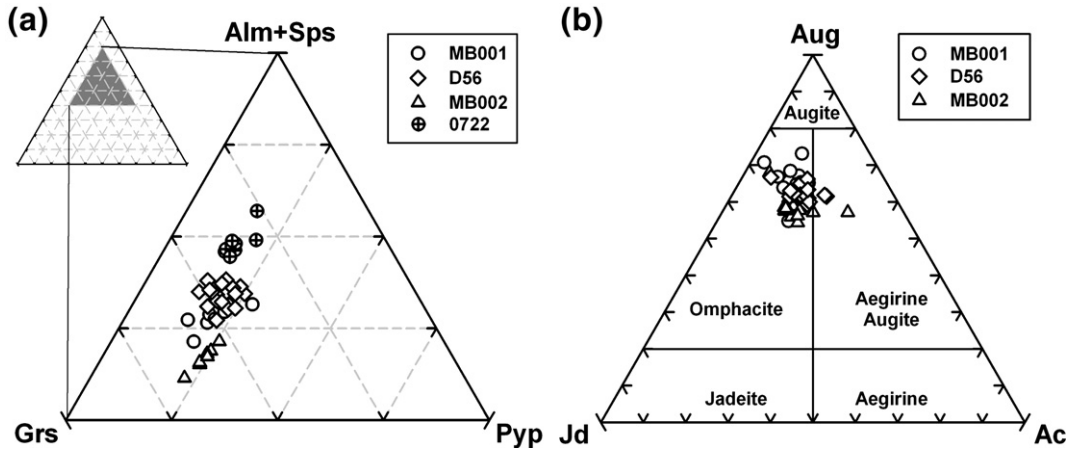

Fig. 3. Compositions of (a) garnet and (b) clinopyroxene in the analyzed eclogites (MB001, MB002 and D56) and garnetite (0722). Abbreviations: Pyp for pyrope; Alm for almandine; Sps for spessartine; Grs for grossular; Ac for acmite; Aug for augite; Jd for jadeite. The classification scheme for clinopyroxene is from Morimoto (1988).

Table 3
Major (in wt.%) and trace element (in ppm) abundances for the high Fe–Ti eclogites and garnetite from Maobei, Sulu UHP metamorphic terrane

Rock type	High Fe–Ti eclogite								
Sample	MB001	D56		MB002			0720		
	Vein-free	Vein-free		Vein-free		Vein-containing	Vein-free		Vein-containing
SiO_2	42.6[a]	41.0[a]	41.1[b]	42.8[a]	42.1[b]	41.7[b]	39.1[a]	38.9[b]	40.9[b]
TiO_2	3.56	3.02	2.94	3.65	3.48	3.37	3.24	3.12	3.35
Al_2O_3	14.6	17.4	17.4	14.2	13.7	15.0	17.2	17.1	13.2
FeO_{tot}	17.1	17.0	16.7	17.0	17.7	17.5	18.7	18.5	19.5
MnO	0.21	0.20	0.22	0.22	0.25	0.26	0.23	0.26	0.27
MgO	6.66	6.31	6.03	6.97	6.61	6.44	6.99	6.69	6.97
CaO	12.3	11.8	11.5	12.5	11.8	11.7	11.5	11.2	11.6
Na_2O	2.37	2.30	1.92	2.45	2.30	1.89	1.74	1.66	1.67
K_2O	–	–	0.01	–	0.02	0.02	–	0.02	0.02
P_2O_5	0.09	0.06	0.03	0.06	0.03	0.04	0.07	0.04	0.05
Total	99.5	99.1	99.7	99.9	99.9	99.8	99.8	99.5	99.8
Sc	61.9	59.9	59.2	71.2	68.3	67.5	69.7	64.0	67.8
Cr	12.7	5.67	6.26	8.47	8.13	7.33	2.98	3.47	3.26
Co	59.8	57.8	59.4	65.6	65.9	63.3	68.2	67.9	71.7
Rb	0.324	0.144	0.115	0.630	0.438	0.591	0.522	0.510	0.461
Ba	11.6	8.50	8.91	12.5	–	14.4	392	459	800
Sr	63.2 (56)	52.9	51.2 (51)	58.3	57.0 (57)	134 (135)	269	261 (255)	241 (236)
Y	12.7 (12.4)	12.5	12.1 (12.9)	11.4	10.6 (11.1)	10.7 (11.4)	11.3	10.6 (11.1)	11.3 (11.8)
Nb	0.63	0.63	0.71	0.36	0.29	0.32	0.24	0.27	0.28
Ta	0.053	0.041	0.041	0.027	0.023	0.018	0.022	0.020	0.020
Ti	20,540 (20,503)	17,390	18,183 (17,625)	21,040	21,370 (20,863)	21,866 (20,320)	19,490	19,310 (18,704)	21,536 (20,083)
Zr	18.6 (18)	15.1	14.9 (16)	14.6	13.3 (13)	13.9 (13)	11.8	11.5 (12)	12.0 (12)
Hf	0.648	0.536	0.552	0.542	0.499	0.507	0.434	0.431	0.452
La	2.30	1.73	1.65	1.44	1.71	2.25	7.28	7.01	11.5
Ce	5.12	3.18	2.85	3.64	3.93	5.28	9.08	8.06	12.6
Pr	0.759	0.462	0.455	0.539	0.602	0.754	1.003	0.947	1.31
Nd	4.00	2.62	2.57	3.08	3.18	4.01	4.59	4.38	5.44
Sm	1.56	1.36	1.35	1.22	1.21	1.31	1.63	1.55	1.68
Eu	0.760	0.780	0.746	0.683	0.664	0.727	0.850	0.819	0.942
Gd	1.92	2.12	1.94	1.64	1.61	1.78	2.14	1.95	2.10
Tb	0.364	0.369	0.370	0.327	0.319	0.333	0.368	0.350	0.363
Dy	2.31	2.28	2.33	2.05	2.02	2.05	2.17	2.10	2.20
Ho	0.483	0.496	0.498	0.435	0.434	0.424	0.450	0.433	0.457
Er	1.29	1.31	1.32	1.17	1.15	1.11	1.19	1.14	1.20
Tm	0.178	0.174	0.182	0.161	0.158	0.151	0.155	0.157	0.165
Yb	1.09	1.08	1.10	0.990	0.975	0.919	0.967	0.962	1.00
Lu	0.160	0.156	0.163	0.146	0.143	0.136	0.139	0.141	0.149
Th	0.434	0.269	0.282	0.139	0.141	0.143	0.272	0.302	0.539
U	0.255	0.199	0.205	0.053	0.049	0.042	0.187	0.202	0.213

[a] Columns in which major and trace element contents were determined by XRF and ICP-MS at NTU. The ICP solutions were 2% HNO_3. Trace element abundances in parentheses were determined by XRF at U. Mass.
[b] Columns in which major elements were analyzed by XRF at U. Mass. Samples were dissolved in 0.1% HF+2% HNO_3 solutions for ICP-MS analysis at NTU. Trace element abundances in parentheses were determined by XRF at U. Mass.
[c] Values for BHVO-1 recommended by Eggins et al. (1997).
[d] Mean values and associated one standard deviation for five BHVO-1 analyses during the sample run.

(Zhang et al., 2004). The compositional differences between these two types of eclogites are important and will be discussed. A third group of CCSD eclogites is compositionally similar to the "high-Ti eclogites" except for lower TiO_2 (~2%); they were referred to as "normal-type eclogites". The fourth group of CCSD eclogites is characterized by high SiO_2 contents of 56–60%; they were classified as "high-Si eclogites" (Zhang et al., 2004).

5.3. Whole-rock isotopic ratios

$^{87}Sr/^{86}Sr$ ratios vary from 0.704211 to 0.705792, and the $^{143}Nd/^{144}Nd$ ratios vary from 0.512405 to 0.513066

Table 3 (*continued*)

Rock type	High Fe–Ti eclogite			Garnetite		
Sample	0717			0722	BHVO-1	
	Vein-free		Vein-containing		Recommended[c] value	Mean[d] (n=5)
SiO_2	38.6[a]	38.2[b]	38.7[b]	32.0[a]		
TiO_2	3.67	3.52	4.02	6.06		
Al_2O_3	17.0	16.9	12.6	19.1		
FeO_{tot}	18.8	18.6	20.9	28.7		
MnO	0.25	0.28	0.29	0.25		
MgO	7.01	6.71	6.99	3.68		
CaO	12.2	11.7	12.0	7.78		
Na_2O	1.78	1.66	1.60	0.49		
K_2O	–	–	0.01	–		
P_2O_5	0.06	0.04	0.15	0.05		
Total	99.4	99.7	99.6	98.1		
Sc	72.3	62.7	67.8	15.7	31.8	32.0±2.6
Cr	3.87	–	–	162	289	278±23
Co	68.7	66.4	69.8	91.6	45	44.8±2.4
Rb	0.126	0.125	0.138	0.350	9.5	9.46±0.45
Ba	14.5	16.5	138	24.7	133	133±9
Sr	50.2	47.0 (46)	81.9 (82)	63.1	390	394±6
Y	11.6	10.8 (11.5)	12.2 (13.6)	7.41	28.0	26.9±0.7
Nb	0.43	0.42	0.41	1.69	19.5	17.2±0.3
Ta	0.030	0.023	0.033	0.035	1.20	1.21±0.04
Ti	22,830	21,623 (21,102)	23,847 (24,100)	33,560	16,610	16,442±1200
Zr	16.2	14.4 (15)	13.0 (14)	11.5	180	175±4
Hf	0.590	0.557	0.494	0.359	4.30	4.33±0.19
La	0.614	0.534	1.36	0.372	15.5	15.9±0.8
Ce	1.71	1.39	3.82	0.457	38.0	39.7±2.4
Pr	0.387	0.345	0.759	0.093	5.45	5.50±0.20
Nd	2.75	2.54	4.69	0.898	24.7	25.3±0.95
Sm	1.53	1.42	1.69	0.936	6.17	6.26±0.23
Eu	0.870	0.782	0.844	0.577	2.06	2.06±0.07
Gd	2.23	1.90	2.13	1.23	6.22	6.27±0.20
Tb	0.383	0.363	0.403	0.232	0.95	1.00±0.03
Dy	2.23	2.18	2.18	1.27	5.25	5.36±0.16
Ho	0.466	0.451	0.465	0.223	1.00	1.02±0.03
Er	1.20	1.16	1.21	0.504	2.56	2.57±0.08
Tm	0.157	0.158	0.167	0.059		0.331±0.010
Yb	0.966	0.944	0.991	0.327	1.98	2.01±0.06
Lu	0.138	0.139	0.139	0.041	0.278	0.280±0.007
Th	0.070	0.067	0.131	0.133	1.26	1.24±0.01
U	0.034	0.035	0.021	0.328	0.420	0.429±0.009

(Table 4). At the time of metamorphism (220 Ma; Li et al., 1993, 2000; Ames et al., 1996), these high Fe–Ti eclogites plot on the mantle array in $^{87}Sr/^{86}Sr$ versus $^{143}Nd/^{144}Nd$ space (Fig. 7), similar to the Bixiling and Maowu eclogites (Chavagnac and Jahn, 1996; Jahn et al., 2003b), thereby implying that the protoliths were mantle-derived.

6. Discussion

Relative to other Dabie–Sulu eclogites, the distinctive features of the high Fe–Ti eclogites are: (1) higher TiO_2, FeO_{total} and lower SiO_2 abundances, (2) lower incompatible element concentrations, and (3) enrichment in Ti and depletion in other HFSEs (Nb, Ta, Zr and Hf) relative to elements with similar compatibilities during mantle melting (Fig. 5). These geochemical features might reflect protolith characteristics or the effects of metamorphism. Protoliths of most eclogites are basalts and gabbros (Jahn, 1998); therefore, comparing the compositions of these high Fe–Ti eclogites to those of basalts and gabbros is a first step to understanding the factors that determined their compositional variations.

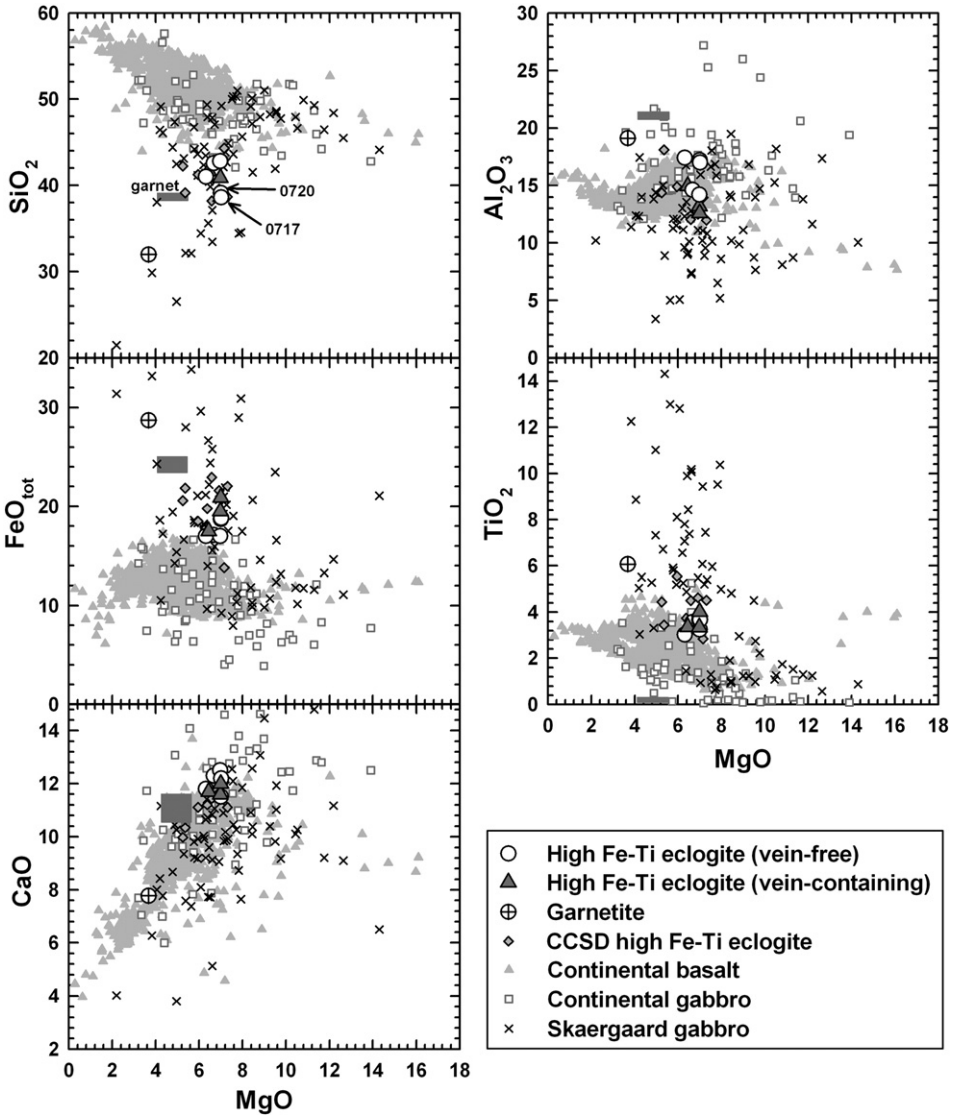

Fig. 4. MgO variation diagrams comparing the Sulu high Fe–Ti eclogites to continental basalts and gabbros. Data of the CCSD eclogites are from Zhang et al. (2004) and Liu et al. (2005a). The rectangular fields represent the compositions of constituent garnet in the studied high Fe–Ti eclogites. Data for continental basalts are from Bose (1973), Shirey et al. (1994), Pik et al. (1999), Hooper (2000), Sano et al. (2001), and Xu et al. (2001). Data for continental gabbros are from Eales and Robey (1976), Weiblen and Morey (1980), Beard and Barker (1989), Klewin (1990), Harris (1995), Abu El-Ela (1996), Arcuri et al. (1998), Kerr et al. (1999), Maier et al. (2000), Schärer et al. (2000), Aït-Djafer et al. (2003), and Kampunzu et al. (2003). Skaergaard gabbros are from McBirney (1998).

6.1. Factors controlling bulk compositions of the analyzed high Fe–Ti eclogites: Protolith or process control?

The negative ε_{Nd} values of most high Fe–Ti eclogites indicate continental affinities (Table 4) and the low incompatible element abundances imply cumulate rather than melt character (Fig. 6). Compared to most continental basalts and gabbros, the analyzed eclogites are lower in SiO_2 but higher in total iron and TiO_2 concentrations at a given MgO content (Fig. 4). Although in MgO variation diagrams these high Fe–Ti eclogites overlap with the Skaergaard ferrogabbros, which contain 2–22 vol.% ilmenite (Fig. 4), three samples, 0717, 0720 and D56, plot off the SiO_2–TiO_2 correlation trend of the Skaergaard ferrogabbros (Fig. 8a). In the SiO_2–Al_2O_3 plot, the vein-free aliquots of samples 0717, 0720 and D56 show the largest deviation from the trend of Skaergaard ferrogabbros. These eclogites are offset toward garnet compositions

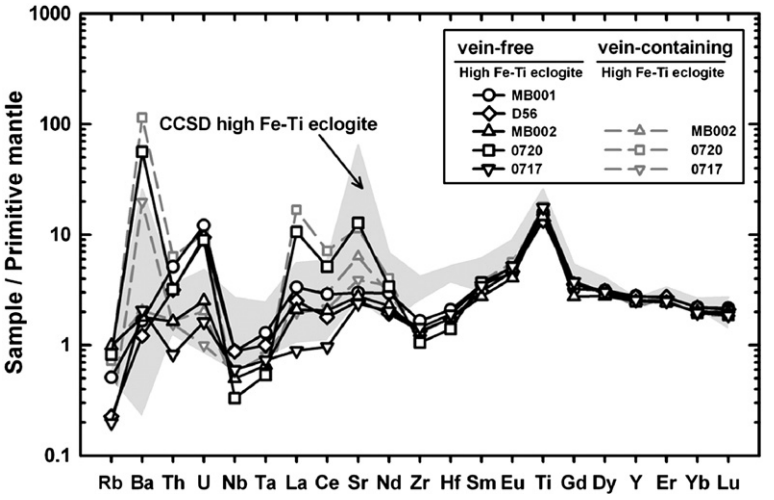

Fig. 5. Abundances of trace elements of the Sulu high Fe–Ti eclogites normalized to the primitive mantle values (Sun and McDonough, 1989), and arranged in an order of increasing compatibility during mantle melting. The grey field is for the CCSD high Fe–Ti eclogites (Zhang et al., 2004). All the high Fe–Ti eclogites show strong enrichment in Ti with depletions in Nb, Ta, Zr and Hf abundances relative to elements of similar compatibilities.

(Fig. 8b), and we infer that they were enriched in garnet as indicated by their high garnet/omphacite ratios (Table 1). In contrast, there is no trend toward rutile composition in the SiO_2–TiO_2 plot (Fig. 8a). The deviation to low SiO_2 contents in the SiO_2–TiO_2 plot, however, cannot be explained by garnet enrichment alone because the trend does not extrapolate to garnet compositions (Fig. 8a). Other processes are also responsible for the low SiO_2 concentrations in these high Fe–Ti eclogites.

Interacting with fluid during metamorphism could decrease SiO_2 concentrations in eclogites. At pressures >10 kbar and temperatures >400 °C, the SiO_2 solubility of fluids is ~2 wt.% for fluid–eclogite equilibration (Manning, 1998) and increases to ~30–40% for fluids interacting with metasediments (Massonne, 1992; Domanik and Holloway, 1998). In contrast, the TiO_2 solubility in fluids is lower with a maximum of 4.7 mmol/kg H_2O (~0.04%) at 1100 °C and 20 kbar (Tropper and Manning, 2005). Within the stability field of eclogites, the TiO_2 mobility is further restricted by low permeability (Van Baalen, 1993). These experiments show that the low SiO_2 contents in eclogites could be partially caused by fluid–eclogite interaction at high

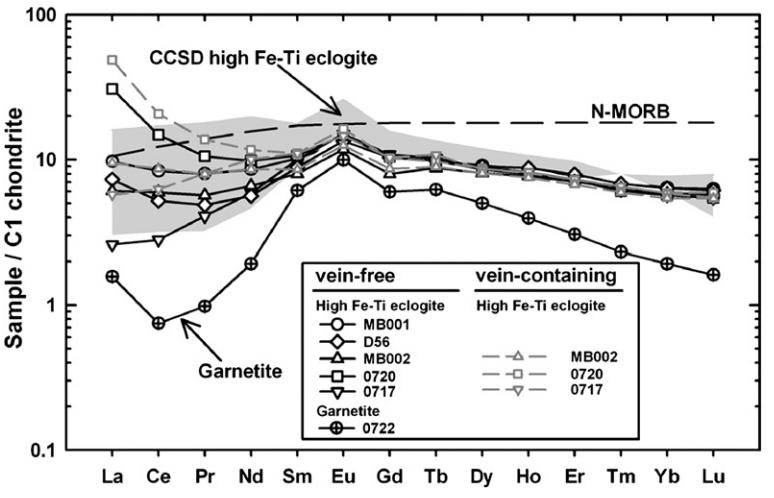

Fig. 6. REE abundances of the Sulu high Fe–Ti eclogites and garnetite normalized to C1 chondrite (Sun and McDonough, 1989). The grey field is for the CCSD high Fe–Ti eclogites (Zhang et al., 2004). The N-MORB average (Sun and McDonough, 1989) is also shown for comparison.

Table 4
Sr and Nd isotopic compositions for the high Fe–Ti eclogites and garnetite from Maobei, Sulu UHP metamorphic terrane

Rock type	High Fe–Ti eclogite					Garnetite
Sample	MB001	MB002	0717	0720	D56	0722
$^{87}Sr/^{86}Sr$	0.705658±18	0.704386±13	0.704211±18	0.705710±11	0.705447±10	0.705792±14
$(^{87}Sr/^{86}Sr)_{220\ Ma}$	0.705612	0.704288	0.704188	0.705688	0.705422	0.705742
$^{143}Nd/^{144}Nd$	0.512471±10	0.512743±10	0.512733±13	0.512405±10	0.512586±12	0.513066±19
$\varepsilon_{Nd}(0)$	−3.3	2.0	1.9	−4.5	−1.0	8.3
$\varepsilon_{Nd}(220\ Ma)$	−4.3	0.86	−2.1	−5.1	−4.3	−3.8

$^{87}Sr/^{86}Sr$ ratios have been corrected for mass fractionation relative to $^{86}Sr/^{88}Sr=0.1194$. $^{143}Nd/^{144}Nd$ ratios have been corrected for mass fractionation relative to $^{146}Nd/^{144}Nd=0.7219$. $^{143}Nd/^{144}Nd=0.512638$ and $^{147}Sm/^{144}Nd=0.196$ for CHUR. The uncertainties are 2σ.

pressures. This process, however, did not affect the TiO_2 concentrations of eclogites. The two low SiO_2 samples, 0717 and 0720, also contain more amphibole (~5 vol.% vs <2 vol.% in other samples) with relatively high Ba/Th and Sr/Nd ratios (Fig. 5), confirming the role of fluid infiltration. In contrast, the absence of significant Ba and Sr enrichments in the high SiO_2 samples indicates limited extents of rock–fluid interaction (Fig. 5).

In summary, the bulk compositions of the analyzed high Fe–Ti eclogites are dominated by protolith characteristics with three of the five samples characterized by some extents of metamorphic modifications. However, it is emphasized that the decoupling between Ti and Nb–Ta–Zr–Hf persists in all analyzed high Fe–Ti eclogites, implying that this feature mainly reflects characteristics of their gabbroic protoliths. In the following sections, the causes of this decoupling are discussed.

6.2. Compositions and proportions of minerals in gabbroic protoliths: Major element constraints

The chemical characteristics of the gabbroic protoliths were controlled by the compositions and proportions of their minerals. We used inferred melt compositions and experimentally determined melt–mineral equilibria to derive compositions of minerals in the gabbroic protoliths. These mineral compositions were then mass balanced using the bulk compositions of

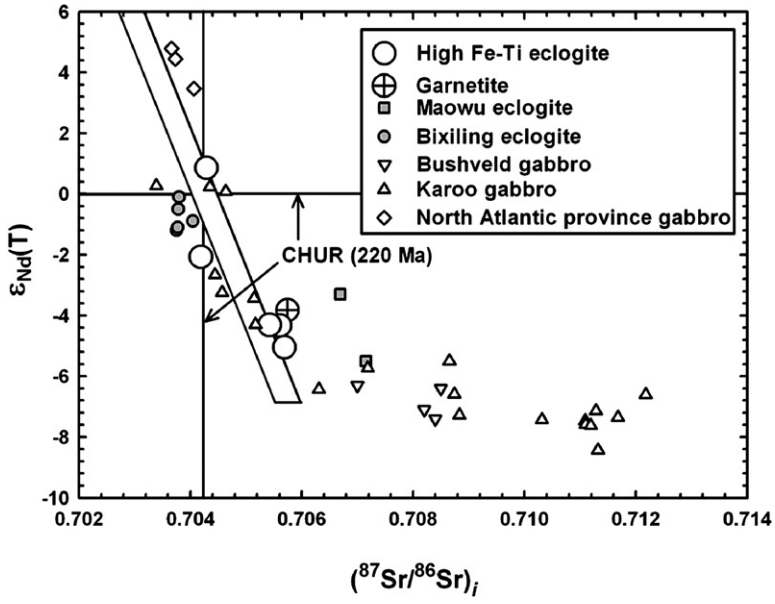

Fig. 7. $\varepsilon_{Nd}(T)$ versus initial $^{87}Sr/^{86}Sr$ plot for the Dabei–Sulu eclogites and continental gabbros. The Sulu high Fe–Ti eclogites, Bixiling eclogites (Chavagnac and Jahn, 1996) and Maowu eclogites (Jahn et al., 2003a,b) were formed at ~220 Ma. The Bushveld gabbros (Maier et al., 2000), Karoo gabbros (Milner and Le Roex, 1996) and North Atlantic province gabbros (Bernstein et al., 1998) are calculated at 2.06 Ga, 20 Ma, and 6 Ma, respectively. The Sulu high Fe–Ti eclogites, Bixiling eclogites and Maowu eclogites have Sr–Nd isotopic compositions similar to those of continental gabbros. The solid lines indicate the chondritic values at 220 Ma. Two sigma errors are smaller than symbol sizes.

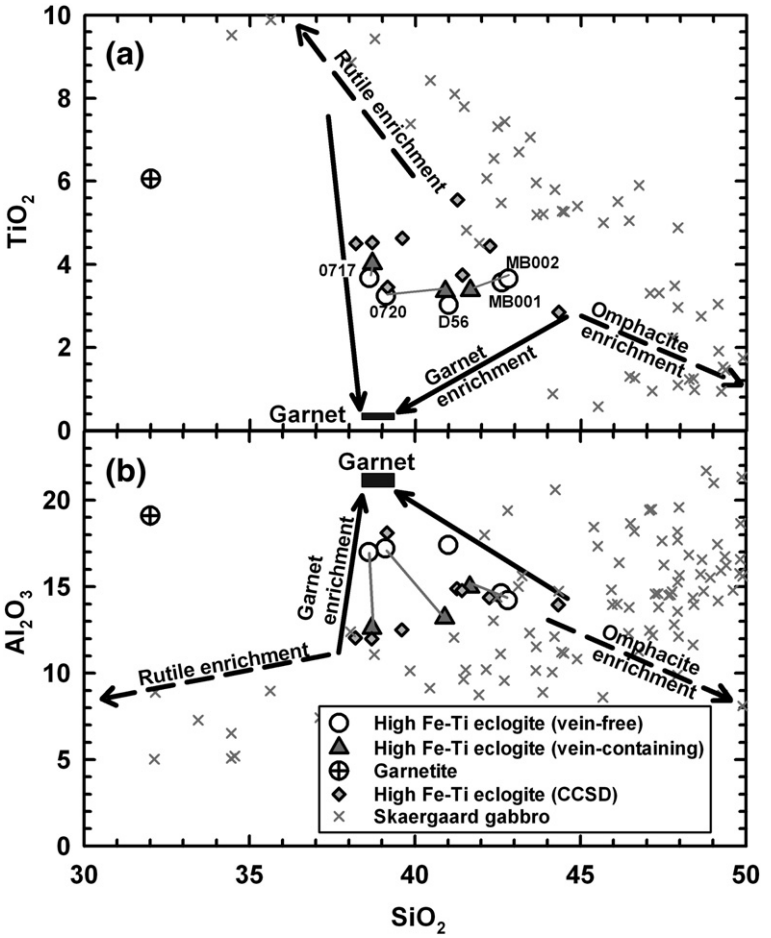

Fig. 8. (a) TiO_2 and (b) Al_2O_3 contents versus SiO_2 content comparing the high Fe–Ti eclogites to the Skaergaard gabbros (McBirney, 1998). The effects of concentrating omphacite and rutile by metamorphic differentiation are shown by two dashed arrow lines, while the effects of garnet enrichment from two different protolith compositions are indicated by two solid arrow lines towards the composition of garnet in the high Fe–Ti eclogites. The vein-free and vein-containing aliquots of a sample are connected by a grey line.

gabbroic protoliths to determine proportions of constituent minerals.

Major and trace element abundances of the analyzed eclogites indicate that their protoliths were Ti-rich gabbros mainly composed of plagioclase, clinopyroxene, olivine and Fe–Ti oxides. We consider that these minerals crystallized from melts having compositions similar to that of the CCSD high-Si, high-Ti and normal type eclogites, which have basaltic compositions with $^{143}Nd/^{144}Nd$ ratios within the range of the high Fe–Ti eclogites (Zhang et al., 2004; Liu et al., 2005b). Most of these CCSD eclogites contain <5% MgO (Zhang et al., 2004); therefore, they could represent melts multiply saturated with plagioclase, clinopyroxene, olivine and Fe–Ti oxides (Toplis and Carroll, 1995). Based on the experimentally determined plagioclase/melt Ca–Na exchange coefficient $[K_D=(Ca/Na)_{plag}/(Ca/Na)_{melt}]$ of 0.8–1.3 (Grove et al., 1992), the plagioclase in equilibrium with the hypothetical melt compositions contains 30–70 mol% anorthite (An_{30-70}). Using the same approach, olivine compositions are inferred to be Fo_{40-70} given the olivine/melt Fe–Mg exchange coefficient $[K_D=(Fe/Mg)_{ol}/(Fe/Mg)_{melt}]$ of 0.29±0.02 (e.g., Gaetani and Watson, 2002). These inferred olivine and plagioclase compositions are similar to those in gabbros forming the Skaergaard layered intrusion (Winter, 2001). Clinopyroxene compositions are complex functions of equilibrium pressure, temperature and melt compositions; therefore, they cannot be readily deduced from clinopyroxene–melt equilibria (Yang et al., 1996; Putirka, 1999; Putirka et al., 2003). However, magmatic clinopyroxene (augite) typically contains ~52% SiO_2, ~1% TiO_2, 2–4% Al_2O_3 and 2–4% Na_2O with MgO, CaO and FeO varying in relatively

Table 5
The results of mass balance using unweighted least squared regression

	Plag	Cpx	Ol	Fe–Ti oxide	Bulk	$\sum R^2$
Composition [a]	An_{60}	mg#=65	Fo_{50}	FeO_{tot}/TiO_2 [b]=0.9	MB002	11
Proportion (%)	38	31	20	8		
Composition [a]	An_{60}	mg#=65	Fo_{50}	FeO_{tot}/TiO_2=3	MB002	1.8
Proportion (%)	41	39	8	12		
Composition [a]	An_{60}	mg#=65	Fo_{50}	FeO_{tot}/TiO_2=3	0717	15
Proportion (%)	48	26	11	15		

[a] See discussion for the choice of mineral compositions.
[b] Weight percent ratio of FeO_{tot}/TiO_2 in Fe–Ti oxide.

larger ranges of 14–19%, 16–22%, and 6–11%, respectively (e.g., Yang et al., 1994, 1999; Batanova et al., 2005). Compositions of Fe–Ti oxides are calculated as mixtures of ilmenite and magnetite. The suitability of these inferred mineral compositions can be evaluated by the following mass balance calculations.

The inferred mineral compositions were used to derive the proportions of minerals in the gabbroic protoliths. To minimize the effects of metamorphic modifications, composition of the high SiO_2 sample, MB002, is considered as the protolith composition. With these compositional parameters, the un-weighted least squared fit resulted in 38% plagioclase, 31% clinopyroxene, 20% olivine, and 8% ilmenite in the gabbroic protoliths with a sum of squared residuals ($\sum R^2$) of 11 (Table 5). Varying the composition of plagioclase, clinopyroxene and olivine within the inferred ranges does not significantly affect the results. However, decreasing TiO_2 content in Fe–Ti oxides from 52% to 25% by increasing magnetite/ilmenite ratio significantly improves $\sum R^2$ from 11 to 1.8 and results in plagioclase:clinopyroxene:olivine:Fe–Ti oxides of 41:39:8:12 (Table 5). Although the $\sum R^2$ of 1.8 is higher than the values of <1 from the mass balance calculations for isothermal crystallization experiments (e.g., Grove et al., 1992, 2003; Yang et al., 1996), it is satisfactory considering the uncertainty in protolith compositions, and the neglect of minor phases in cumulates, such as apatite. A high $\sum R^2$ of 15 is obtained if the compositions of low SiO_2 samples 0717 and 0720 are considered as protolith compositions (Table 5), confirming our choice of high SiO_2 sample, MB002, as an approximation for protolith composition and our inference that low SiO_2 samples (0717 and 0720) were subjected to metamorphic modifications. The inferred mineral proportions are in the ranges for Skaergaard gabbros (Conrad and Naslund, 1989) and the plagioclase/clinopyroxene ratios of ~1 are consistent with crystallization at 2–8 kbar (Grove et al., 1992). The modeled mineral proportions for the gabbroic protoliths (plagioclase:clinopyroxene:olivine:Fe–Ti oxides=41:39:8:12) form the basis for modeling trace element variations in the analyzed eclogites.

6.3. Trace element compositions of the protoliths: Constraints from crystallization modeling

Trace element compositions of the gabbroic protoliths can be inferred from parental melt compositions using bulk solid/melt partition coefficients ($D_i^{solid/melt}$ with subscript i indicating an element of interest). The bulk $D_i^{solid/melt}$ is calculated from $D_i^{mineral/melt}$ (Table 6) and mineral proportions deduced in the preceding section (Table 5). As for inferring the major element compositions of minerals in the gabbroic protoliths, the trace element abundances of CCSD high-Si, high-Ti and normal type eclogites are considered as analogs of melt compositions (Zhang et al., 2004).

Table 6
Partition coefficients for model calculations

	pl/melt [a]	cpx/melt [b]	mt/melt [c]	ilm/melt [d]	Fe–Ti oxide/melt [e] (mt/ilm=1)
Nb	0.016	0.0077	0.4	0.8	0.6
Ta	0.016	*0.0077* [f]	*0.4*	*0.8*	0.6
La	0.141	0.0536	0.0029	0.0072	0.0051
Ce	0.095	0.0858	*0.0038*	*0.0076*	0.0057
Sr	1.5	0.1283	0.008	0.008	0.008
Nd	0.074	0.1873	*0.0055*	*0.0084*	0.0069
Zr	0.00272	0.1234	0.1	0.33	0.22
Hf	*0.00272*	0.256	*0.1*	0.419	0.260
Sm	0.077	0.27	0.0072	0.0091	0.0082
Eu	0.0623	*0.43*	*0.0064*	*0.0084*	0.0074
Ti	0.0572	0.384	–	17 [g]	8.3 [h]
Gd	*0.0557*	*0.44*	0.0055	0.0077	0.0066
Dy	*0.0424*	0.442	*0.01*	*0.0137*	0.0118
Y	0.0227	0.467	0.0039	0.0045	0.0042
Er	*0.0202*	0.387	*0.0148*	*0.0197*	0.0172
Yb	*0.0159*	0.43	*0.0203*	*0.0257*	0.0230
Lu	*0.0093*	0.433	0.023	0.029	0.026

[a] Bindeman and Davis (2000).
[b] Hart and Dunn (1993), Hauri et al. (1994).
[c] Nielsen et al. (1992), Pearce and Norry (1979).
[d] Nielsen et al. (1992), McKay et al. (1986).
[e] The values for Fe–Ti oxides containing equal molar proportions of ilmenite and magnetite.
[f] Numbers in italic are inferred from ionic radius. Variations in values for HREE of pl/melt and Fe–Ti oxide/melt do not affect the model results for the strong control of cpx on HREE.
[g] Calculated by dividing the TiO_2 content of ilmenite (~51%) by that of basaltic melts (3%).
[h] Calculated by dividing the TiO_2 content of Fe–Ti oxides with mt/ilm ratio of 1 (~25%) by that of basaltic melts (3%).

The modeled gabbros are characterized by positive Ti anomalies and Nb–Ta–Zr–Hf depletions, consistent with the variation patterns of the analyzed high Fe–Ti eclogites (Fig. 9). In detail, the modeled gabbro in equilibrium with the melt having the composition of CCSD normal-type eclogite, sample B990R636P20i, provides the best fits to trace element concentrations of the analyzed eclogites (Fig. 9a). Using the compositions of CCSD high-Ti eclogites as parental melt compositions produces cumulates with HREE abundances ~30% lower and Sr contents ~2–3 times higher than the analyzed eclogites (Fig. 9b). These discrepancies

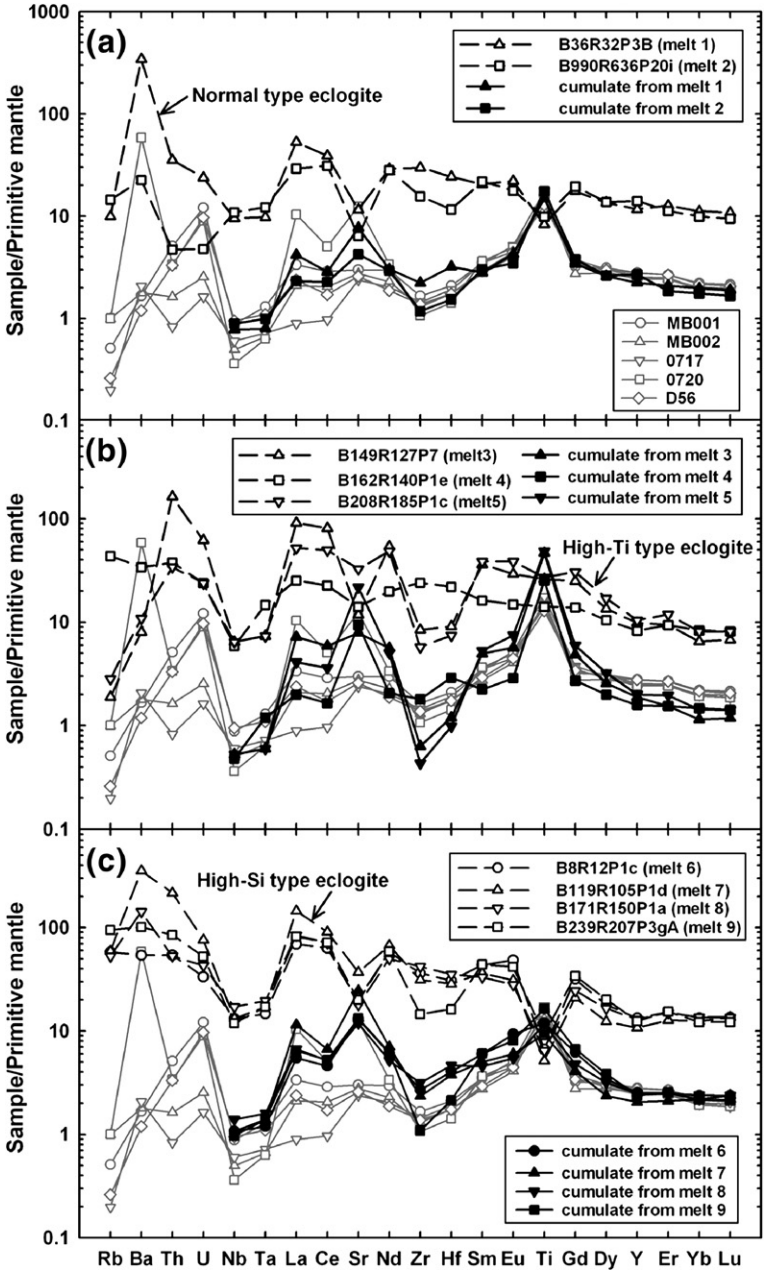

Fig. 9. Primitive mantle (Sun and McDonough, 1989) normalized trace element abundances of CCSD (a) normal type eclogites, (b) high-Ti type eclogites, (c) high-Si type eclogites, and the modeled cumulates crystallized from melts having compositions of these CCSD eclogites (Zhang et al., 2004). The modeled gabbros have positive Ti anomalies with depletions in Nb, Ta, Zr and Hf contents, similar to the variation patterns of the analyzed high Fe–Ti eclogites (grey symbols). The legends denote the sample numbers of the CCSD eclogites and their corresponding cumulates. For clarity, only the vein-free aliquots of the analyzed samples are plotted.

are minor if the effects of metamorphism on Sr contents and the uncertainties in partition coefficients are considered. Therefore, it is suggested that melts with compositions similar to the CCSD high-Ti eclogites can also be parental melts of the gabbroic protoliths of the high Fe–Ti eclogites. Gabbros coexisting with melts having the compositions of CCSD high-Si eclogites do not provide good fits; these melts have higher LREE, MREE and HFSE contents (Fig. 9c), possibly because these high-Si eclogites were subjected to metamorphic modifications on their protolith compositions as indicated by their petrographic textures and high SiO_2 contents of 56–60% (Zhang et al., 2004). Varying plagioclase and clinopyroxene proportions (up to 5%) does not significantly affect the results. Models of equilibrium crystallization and fractional crystallization lead to similar trace element compositions in cumulates. The analyzed eclogites with highest SiO_2 concentrations (MB001 and MB002) have trace element abundances most comparable to that of the modeled cumulates (Fig. 9a). In contrast, the LREE concentrations of two low SiO_2 samples, 0717 and 0720, deviate from the model cumulates (Fig. 9a), consistent with the prior inference that these two samples were subjected to metamorphic modifications. Although using eclogite compositions as analogs of basaltic protolith compositions for crystallization modeling ignores the chemical effects of metamorphism, we have successfully produced the uncommon feature of Ti enrichment associated with Nb–Ta–Zr–Hf depletions in the analyzed eclogites. The results, therefore, imply that the protolith compositions were not intensively modified by metamorphism and the observed HFSE decoupling mainly reflects protolith characteristics. More significantly, based on our model calculations, we suggest that the CCSD high Fe–Ti eclogites (subunit 8) with compositions similar to our analyzed samples can be related to the overlying normal type and probably high-Ti type eclogites (subunits 4 and 6) by crystal fractionation. This implies the existence of a layered intrusion within the subducted continent prior to subduction.

6.4. Causes of decoupling between Ti and other HFSEs

The feature of Ti-enrichment accompanied by Nb, Ta, Zr and Hf depletions in the analyzed eclogites is not expected, because HFSEs typically behave coherently during magmatic processes and are concentrated into Fe–Ti oxides. Specifically, $D^{\text{Fe–Ti oxides/basalt}}_{\text{Ti, Nb, Ta}}$ are at least 20 times greater than $D^{\text{clinopyroxene/basalt}}_{\text{Ti, Nb, Ta}}$ and $D^{\text{plagioclase/basalt}}_{\text{Ti, Nb, Ta}}$, whereas $D^{\text{Fe–Ti oxide/basalt}}_{\text{Zr, Hf}}$ exceed $D^{\text{clinopyroxene/basalt}}_{\text{Zr, Hf}}$ by lesser extents, factors of <3 (Table 6). Therefore, Fe–Ti oxides in cumulate rocks affect Ti, Nb and Ta more strongly than Zr and Hf. For example, addition of 2% ilmenite to cumulates leads to a 2–3 fold increase in the Ti/Eu and Nb/La ratios while the Zr/Nd ratio only increases by ~10%. Given these constraints of HFSE crystal/melt partitioning, the melts in equilibrium with gabbros having Ti-enrichment accompanied by Nb, Ta, Zr and Hf depletions must (1) evolve to saturation of Fe–Ti oxides, (2) have Ti/Eu ratios close to the chondritic value, and (3) be strongly depleted in Nb, Ta, Zr and Hf relative to elements with similar compatibilities during mantle melting. The compositions of CCSD normal type and high-Ti type eclogites (Zhang et al., 2004) satisfy all these three requirements (Fig. 9a,b). Saturation of Fe–Ti oxides can occur in evolved basalts erupted in all tectonic settings (Leeman et al., 1976; Frey et al., 1990; Hooper and Hawkesworth, 1993; Yang et al., 1998). However, prominent Nb–Ta–Zr–Hf depletions associated with subtle (or absence of) Ti depletion mainly occur in subduction zone lavas and basalts that were intensively contaminated by continental crust (e.g., Hansen and Nielsen, 1999; Kent et al., 2002). The inference of relating arc lavas and high Fe–Ti-gabbros characterized by the observed HFSE decoupling is supported by the occurrences of such gabbros in the ancient arc system in south-central Alaska (Greene et al., 2006) and in the Eastern Desert of Egypt (Abu El-Ela, 1996). Although Ti enrichment with Nb–Ta–Zr–Hf depletions is not a common feature in continental gabbros, an alternative hypothesis is that these high Fe–Ti eclogites are metamorphosed crustally contaminated continental gabbros. If the protoliths of the high Fe–Ti eclogites were formed at 700–850 Ma as that of most Dabie–Sulu eclogites, an arc origin for these protoliths is consistent with the model that postulated the Yangtze block was isolated from the super Rodinia continent by arc belts (Zhou et al., 2002). However, this does not preclude plume-related magmatism within the interior of the Yangtze block during 700–850 Ma.

6.5. Is the high TiO_2 (>5%) in CCSD eclogites magmatic or metamorphic in origin?

The CCSD eclogites cored at the depth range of 530–600 m (subunit 8) are compositionally similar to our analyzed eclogites. Nevertheless, some of these CCSD high Fe–Ti eclogites have TiO_2 concentrations up to 4–6%, even higher than that, 3.5%, of the analyzed eclogites. Toplis and Carroll (1995) experimentally showed that the mineral assemblage in equilibrium with

melts having major oxide abundances similar to that of the hypothetical melts in our model contains up to 9% ilmenite, contributing 4.5% TiO_2 to bulk mineral assemblage. Taking the contribution of 30–40% clinopyroxene (~0.6–1% TiO_2) into account, the TiO_2 content in the bulk crystallized mineral assemblage is estimated to be ~5%. Such high TiO_2 abundances also occur in ferrogabbros from the Kiglapait and Skaergaard intrusions with up to 7% and 13% TiO_2, respectively (Morse, 1981; McBirney, 1998). Therefore, gabbroic cumulates predicted from crystallization experiments and natural examples indicate that high TiO_2 contents of 4–6% in the CCSD high Fe–Ti eclogites could be derived from basalts with <4.5% TiO_2. The analyzed garnetite also contains high TiO_2 concentration of 6.06% reflecting the role of Fe–Ti oxides. The mechanism of involving a high proportion (~15%) of Fe–Ti oxides in the garnetite is beyond the scope of this paper and remains as a subject for further investigation.

The CCSD subunits 4 and 6 eclogites cored at depth ranges of 318–380 and 420–470 m also contain 2–6% TiO_2 (Zhang et al., 2004). Unlike the analyzed samples and CCSD subunit 8 eclogites (Zhang et al., 2004), these eclogites, referred to as high-Ti eclogites, show neither Ti-enrichment nor HFSE decoupling (Fig. 9b). In addition, their incompatible element concentrations are ~3–8 times higher than that of the analyzed eclogites but comparable to that of basalts erupted at various tectonic environments. However, some of these high-Ti eclogites contain TiO_2 abundances of 4–6%, which are uncommonly high for basalts. The liquid line of descent (LLD) for fractional crystallization of basalts indicates that primitive basaltic magmas increase in TiO_2 with decreasing MgO contents during early stages of olivine–plagioclase–augite fractionation. Then, Fe–Ti oxides become saturated as basalts evolve to ~4–5% MgO and ~4.5% TiO_2. Further crystallization of Fe–Ti oxides decreases the TiO_2 concentrations in residual melts (Leeman et al., 1976; Frey et al., 1990; Yang et al., 1998). Moreover, the jotunitic magma that precipitated world-class ilmenite deposits in Norway contains only 3–4% TiO_2 (Duchesne, 1999). Therefore, the high TiO_2 concentrations of 5–6% in the CCSD high-Ti eclogites cannot be readily explained by reflecting compositions of basaltic protoliths. Instead, concentrating rutile by metamorphic differentiation is a more plausible interpretation for the high TiO_2 abundances of >5% in these high-Ti eclogites. This inference needs to be confirmed by high-resolution analyses on CCSD eclogites, an important approach for understanding the compositional diversity of eclogites from the Sulu metamorphic terrane.

7. Conclusions

The compositions of high Fe–Ti eclogites from Maobei in the Sulu metamorphic terrane in eastern China mainly reflect protolith characteristics, although the effects of metamorphic differentiation and fluid infiltration can be detected. The important compositional features and associated implications include the following.

(1) Major element abundances of the high Fe–Ti eclogites are comparable to that of Skaergaard gabbros. However, some analyzed samples deviate from the SiO_2–Al_2O_3 and SiO_2–TiO_2 correlations of the Skaergaard gabbros reflecting garnet enrichment and fluid infiltration during metamorphism.
(2) Trace element abundances of the analyzed eclogite samples are comparable to those of gabbros indicating gabbroic protoliths. Mass balance using major oxides constrains the mineral proportions in the gabbroic protoliths to be 41% plagioclase, 39% clinopyroxene, 8% olivine, and 12% Fe–Ti oxides. The ratio of plagioclase/clinopyroxene is consistent with crystallization at 2–8 kbar.
(3) The HFSEs in the analyzed eclogites are decoupled; specifically, Ti enrichment is accompanied by Nb–Ta–Zr–Hf depletions. Gabbros with such features can only be crystallized from melts depleted in Nb, Ta, Zr and Hf with Ti/Eu ratios close to the chondritic value. These are characteristics of arc lavas and continental basalts subjected to crustal contamination.
(4) The REE and HFSE abundances of the analyzed high Fe–Ti eclogites are similar to that of the CCSD eclogites cored at 530–600 m (subunit 8) and can be modeled as cumulates from melts compositionally similar to the CCSD eclogites cored at shallower levels of 318–380 and 420–470 m (subunits 4 and 6). This result implies a layered intrusion in the continent prior to collision and subduction.
(5) Some of the CCSD subunits 4 and 6 eclogites contain >5% TiO_2, which cannot be produced by magmatic processes. They must result from metamorphic enrichment of rutile.

Finally, high Fe–Ti eclogites also occur at Pianpaludo in Italy, Sunnfjord in Norway, and Shubino Village in USSR (summarized in Force, 1991). As in the Sulu terrane, these eclogites have also been explored for mining titanium. However, the trace element characteristics of these

eclogites have not been investigated. If these eclogites also have decoupled HFSE abundances, such as the high Ti/Zr ratios of >1000 in the studied eclogites, the geochemical effects of recycling these eclogites into the mantle may be significant.

Acknowledgment

We benefit from the discussion with Professor Bor-Ming Jahn whose comments stimulated our thinking and improved our data interpretation. We are in debted to the following laboratory managers for their assistance in chemical analyses; Yoshiyuki Iizuka for EPMA, Chi-Yu Lee for XRF, Mei-Fei Chu for ICP-MS, and Li-Yun Huang for Sr–Nd isotopic analyses. Special thanks to Michael Rhodes for the access to his XRF facilities. We thank Wei-Min Chen and Tiannan Yang for their guidance during the field trips for sample collections. We are grateful to Frederick Frey for his scientific comments and improving our presentation. Critical comments from two anonymous reviewers and the editorial efforts of Roberta Rudnick are highly appreciated. This research is supported by the NSC grants, NSC91-2116-M006-005 to H.-J. Yang and NSC93-2116-M006-004 to S.-C. Yu.

References

Abu El-Ela, F.F., 1996. The petrology of the Abu Zawal gabbroic intrusion, Eastern Desert, Egypt: an example of an island-arc setting. J. Afr. Earth Sci. 22, 147–157.

Aït-Djafer, S., Ouzegane, K., Paul-Liégeois, J., Kienast, J.R., 2003. An example of post-collisional mafic magmatism: the gabbro–anorthosite layered complex from the Tin Zebane area (western Hoggar, Algeria). J. Afr. Earth Sci. 37, 313–330.

Ames, L., Zhou, G., Xiong, B., 1996. Geochronology and isotopic character of ultrahigh-pressure metamorphism with implications for collision of the Sino–Korean and Yangtze Cratons, central China. Tectonics 15, 472–489.

Arcuri, T., Ripley, E.M., Hauck, S., 1998. Sulfur and oxygen isotope studies of the interaction between pelitic xenoliths and basaltic magma at the Babbitt and serpentine Cu–Ni deposits, Duluth complex, Minnesota. Econ. Geol. 93, 1063–1075.

Batanova, V.G., Pertsev, A.N., Kamenetsky, V.S., Ariskin, A.A., Mochalov, A.G., Sobolev, A.V., 2005. Crustal evolution of island-arc ultramafic magma: Galmoenan pyroxenite–dunite plutonic complex, Koryak highland (far east Russia). J. Petrol. 46, 1345–1366.

Beard, J.S., Barker, F., 1989. Petrology and tectonic significance of gabbros, tonalities, shoshinites, and anorthosites in a late Paleozoic arc–root complex in the Wrangellia terrane, southern Alaska. J. Geol. 97, 667–683.

Bernstein, S., Keleman, P.B., Tegner, C., Kurz, M.D., 1998. Post-breakup basaltic magmatism along the East Greenland tertiary rifted margin. Earth Planet. Sci. Lett. 160, 845–862.

Bindeman, I.N., Davis, A.M., 2000. Trace element partitioning between plagioclase and melt: investigation of dopant influence on partition behavior. Geochim. Cosmochim. Acta 64, 2863–2878.

Bose, M.K., 1973. Petrology and geochemistry of the igneous complex of Mount Girnar, Gujarat, India. Contrib. Mineral. Petrol. 39, 247–266.

Chavagnac, V., Jahn, B.M., 1996. Coesite-bearing eclogites from the Bixiling Complex, Dabie Mountains, China: Sm–Nd ages, geochemical characteristics and tectonic implications. Chem. Geol. 133, 29–51.

Chung, S.L., Liu, D.Y., Ji, J.Q., Chu, M.F., Lee, H.Y., Wen, D.J., Lo, C.H., Lee, T.Y., Qian, Q., Zhang, Q., 2003. Adakites from continental collision zones: melting of thickened lower crust beneath sourthern Tibet. Geology 31, 1021–1024.

Conrad, M.E., Naslund, H.R., 1989. Modally-graded rhythmic layering in the Skaergaard intrusion. J. Petrol. 30, 251–269.

Domanik, K.J., Holloway, J.R., 1998. Experimental determination of the stability and phase relations of phengitic muscovite in a calcareous metapelite from the Dabie Mountains, China. International Workshop on UHP Metamorphism and Exhumation, Abstract, pp. 206–207.

Duchesne, J.C., 1999. Fe–Ti deposits in Rogaland anorthosites (South Norway): geochemical characteristics and problems of interpretation. Miner. Depos. 34, 182–198.

Eales, H.V., Robey, J.V.A., 1976. Differentiation of tholeiitic Karoo magma at Birds River, South Africa. Mineral. Petrol. 56, 101–117.

Eggins, S.M., Woodhead, J.D., Kinsley, L.P.J., Mortimer, G.E., Sylvester, P., McCulloch, M.T., Hergt, J.M., Handler, M.R., 1997. A simple method for the precise determination of 40 trace elements in geological samples by ICPMS using enriched isotope internal standardisation. Chem. Geol. 134, 311–326.

Force, E.R., 1991. Geology of titanium-mineral deposits. Spec. Pap. - Geol. Soc. Am. 259, 14–16.

Frey, F.A., Wise, W.S., Garcia, M.O., West, H., Kwon, S.-T., Kennedy, A., 1990. Evolution of Mauna Kea volcano, Hawaii: petrologic and geochemical constraints on postshield volcanism. J. Geophys. Res. 95, 1271–1300.

Gaetani, G.A., Watson, E.B., 2002. Modeling the major-element evolution of olivine-hosted melt inclusions. Chem. Geol. 183, 25–41.

Goldstein, J.I., Newbury, D.E., Echlin, P., Joy, D.C., Fiori, F., Lifshin, E., 1981. Scanning Electron Microscopy and X-ray Microanalysis. Plenum Press, New York.

Greene, A.R., DeBari, S.M., Kelemen, P.B., Blusztajn, J., Clift, P.D., 2006. A detailed geochemical study of Island arc crust: the Talkeetna arc section, south-central Alaska. J. Petrol. 47, 1051–1093.

Grove, T.L., Kinzler, R.J., Bryan, W.B., 1992. Fractionation of mid-ocean ridge basalt (MORB). Am. Geophys. Union, Geophys. Monogr. 71, 281–310.

Grove, T.L., Elkins-Tanton, L.T., Parman, S.W., Chatterjee, N., Muntener, O., Gaetani, G.A., 2003. Fractional crystallization and mantle-melting controls on calc-alkaline differentiation trends. Contrib. Mineral. Petrol. 145, 515–533.

Hansen, H., Nielsen, T.F.D., 1999. Crustal contamination in Palaeogene East Greenland flood basalts: plumbing system evolution during continental rifting. Chem. Geol. 157, 89–118.

Harris, C., 1995. Oxygen isotope geochemistry of the Mesozoic anorogenic complexes of Damaraland, northwest Namibia: evidence for crustal contamination and its effect on silica saturation. Contrib. Mineral. Petrol. 122, 308–321.

Hart, S.R., Dunn, T., 1993. Experimental cpx/melt partitioning of 24 trace elements. Contrib. Mineral. Petrol. 113, 1–8.

Hauri, E.H., Wagner, T.P., Grove, T.L., 1994. Experimental and natural partitioning of Th, U, Pb and other trace elements between garnet, clinopyroxene and basaltic melts. Chem. Geol. 117, 149–166.

Hirschmann, M.M., Stopler, E., 1996. A possible role of garnet pyroxenite in the origin of the 'garnet signature' in the MORB. Contrib. Mineral. Petrol. 124, 185–208.

Hooper, P.R., 2000. Chemical discrimination of Columbia river basalt flows. Geochem. Geophys. Geosyst. 1. doi:10.1029/2000GC000040.

Hooper, P.R., Hawkesworth, J., 1993. Isotopic and geochemical constraints on the origin and evolution of the Columbia River basalt. J. Petrol. 34, 1203–1246.

Huang, S., Frey, F.A., 2005. Recycled oceanic crust in the Hawaiian plume: evidence from temporal geochemical variations within the Koolau Shield. Contrib. Mineral. Petrol. 149, 556–575.

Jahn, B.M., 1998. Geochemical and isotopic characteristics of UHP eclogites and ultramafic rocks of the Dabie orogen: implications for continental subduction and collisional tectonics. In: Backer, B., Liou, J.G. (Eds.), When Continents Collide: Geodynamics and Geochemistry of Ultrahigh-pressure Rocks, vol. 10, pp. 203–239.

Jahn, B.M., Rumble, D., Liou, J.G., 2003a. Geochemistry and isotope tracer study of UHP metamorphic rocks. In: Carswell, A.D., Compagnoni, R. (Eds.), Ultrahigh Pressure Metamorphism: EMU Notes in Mineralogy, vol. 5, pp. 365–414.

Jahn, B.M., Fan, Q., Yang, J.J., Henin, O., 2003b. Petrogenesis of the Maowu pyroxenite–eclogite body from the UHP metamorphic terrane of Dabieshan: chemical and isotopic constraints. Lithos 70, 243–267.

Jahn, B.M., Liu, X., Yui, T.F., Morin, N., Coz, M.B.-L., 2005. High-pressure/ultrahigh- pressure eclogites from the Hong'an block, east-central China: geochemical characterization, isotope disequilibrium and geochronological controversy. Contrib. Mineral. Petrol. 149, 499–526.

Kampunzu, A.B., Tombale, A.R., Zhai, M., Bagai, Z., Majaule, T., Modisi, M.P., 2003. Major and trace element geochemistry of plutonic rocks from Francistown, NE Botswana: evidence for a Neoarchaean continental active margin in the Zimbabwe craton. Lithos 71, 431–460.

Kent, A.J.R., Baker, J.A., Wiedenbeck, M., 2002. Contamination and melt aggregation processes in continental flood basalts: constraints from melt inclusions in Oligocene basalts from Yemen. Earth Planet. Sci. Lett. 202, 577–594.

Kerr, A.C., Kent, R.W., Thomson, B.A., Seedhouse, J.K., 1999. Geochemical evolution of the Tertiar Mull volcano, western Scotland. J. Petrol. 40, 873–908.

Klewin, K.W., 1990. Petrology of the Proterozoic Potato River layered intrusion, northern Wisconsin, USA. J. Petrol. 31, 1115–1140.

Leeman, W.P., Vitaliano, G.J., Prinz, M., 1976. Evolved lavas from the Snake River Plain: craters of the Moon National Monument, Idaho. Contrib. Mineral. Petrol. 56, 35–60.

Leitch, A.M., Davies, G.F., 2001. Mantle plumes and flood basalts: enhanced melting from plume ascent and an eclogite component. J. Geophys. Res. 106, 2047–2059.

Li, S., Xiao, Y., Liu, D., Chen, Y., Ge, N., Zhang, R., Hart, S.R., Wang, S., 1993. Collision of the North China and Yangtze blocks and formation of coesite-bearing eclogites: timing and processes. Chem. Geol. 109, 89–111.

Li, S., Jagoutz, E., Chen, Y., Li, Q., 2000. Sm–Nd and Rb–Sr isotopic chronology and cooling history of ultrahigh pressure metamorphic rocks and their country rocks at Shuanghe in the Dabie Mountains, central China. Geochim. Cosmochim. Acta 64, 1077–1093.

Li, Z.X., Li, X.H., Kinny, P.D., Wang, J., Zhang, S., Zhou, H., 2003. Geochronology of Neoproterozoic syn-rift magmatism in the Yangtze Craton, South China and correlations with other continents: evidence for a mantle superplume that broke up Rodinia. Precambrian Res. 122, 85–109.

Liu, Y.S., Zhang, Z.M., Lee, C.T., Gao, S., Zong, K.Q., 2005a. Decoupled high-Ti from low-Nb (Zr) of eclogites from the CCSD: implications for magnetite fractional crystallization in basalt chamber. Acta Pet. Sin. 21, 339–346 (in Chinese with English abstract).

Liu, F.L., Xue, H.M., Meng, F.C., Xu, Z.Q., Li, T.F., Chen, S.Z., 2005b. Sm–Nd dating of eclogites from the main drill hole of the Chinese Continental Scientific Drilling Project and outcrops in the southwestern Sulu Terrane, eastern China. Geol. Chin. 32, 195–204.

Maier, W.D., Arndt, N.T., Curl, E.A., 2000. Progressive crustal contamination of the Bushveld complex: evidence from Nd isotopic analyses of the cumulate rocks. Contrib. Mineral. Petrol. 140, 316–327.

Manning, C.E., 1998. Fluid composition at the blueschist–eclogite transitions in the model system Na_2O–MgO–Al_2O_3–SiO_2–H_2O–HCl. Schweiz. Mineral. Petrogr. Mitt. 78, 225–242.

Massonne, H.J., 1992. Evidence for low-temperature ultrapotassic siliceous fluids in subduction zone environment in the system K_2O–MgO–Al_2O_3–SiO_2–H_2O (KMASH). Lithos 28, 421–434.

McBirney, A.R., 1998. The Skaergaard layered series. Part V. Included trace elements. J. Petrol. 39, 255–276.

McKay, G., Wagstaff, J., Yang, S.R., 1986. Zirconium, hafnium, and rare earth element partition coefficients for ilmenite and other minerals in high-Ti lunar mare basalts: an experimental study. J. Geophys. Res. 91, 229–237.

Milner, S.C., Le Roex, A.P., 1996. Isotope characteristics of the Okenyenya igneous complex, northwestern Namibia: constraints on the composition of the early Tristan plume and the origin of the EM1 mantle component. Earth Planet. Sci. Lett. 141, 277–291.

Morimoto, N., 1988. Nomenclature of pyroxenes. Schweiz. Mineral. Petrogr. Mitt. 68, 95–111.

Morse, S.A., 1981. Kiglapait geochemistry IV: the major elements. Geochim. Cosmochim. Acta 45, 461–479.

Münker, C., 1998. Nb/Ta fractionation in a Cambrian arc/back arc system, New Zealand: source constraints and application of refined ICPMS technique. Chem. Geol. 144, 23–45.

Nielsen, R.L., Gallahan, W.E., Newberger, F., 1992. Experimentally determined mineral–melt partition coefficients for Sc, Y and REE for olivine, orthopyroxene, pigeonite, magnetite and ilmenite. Contrib. Mineral. Petrol. 110, 488–499.

Pearce, J.A., Norry, M.J., 1979. Petrogenetic implications of Ti, Zr, Y, and Nb variations in volcanic rocks. Contrib. Mineral. Petrol. 69, 33–47.

Pik, R., Deniel, C., Coulon, C., Yirgu, G., Marty, B., 1999. Isotopic and trace element signatures of Ethiopian flood basalts: evidence for plume–lithosphere interactions. Geochim. Cosmochim. Acta 63, 2263–2279.

Putirka, K., 1999. Clinopyroxene+liquid equilibrium to 100 kbar and 2450 °K. Contrib. Mineral. Petrol. 135, 151–163.

Putirka, K., Mikaelian, H., Ryerson, F., Shaw, H., 2003. New clinopyroxene–liquid thermobarometers for mafic, evolved, and volatile-bearing lava compositions, with applications to lavas from Tibet and the Snake River Plain, Idaho. Am. Mineral. 88, 1542–1554.

Rhodes, J.M., Vollinger, M.J., 2004. Composition of basaltic lavas sampled by phase-2 of the Hawaii Scientific Drilling Project: geochemical stratigraphy and magma types. Geochem. Geophys. Geosyst. 5, Q03G13. doi:10.1029/ 2002GC000434.

Rudnick, R.L., Barth, M., Horn, I., McDonough, W.F., 2000. Rutile-bearing refractory eclogites: missing link between continents and depleted mantle. Science 287, 278–281.

Sano, T., Fujii, T., Deshmukh, S.S., Fukuoka, T., Aramaki, S., 2001. Differentiation process of Deccan Trap basalts: contribution from geochemistry and experimental petrology. J. Petrol. 42, 2175–2195.

Schärer, U., Girardeau, J., Cornen, G., Boillot, G., 2000. 138–121 Ma asthenospheric magmatism prior to continental break-up in the North Atlantic and geodynamic implications. Earth Planet. Sci. Lett. 181, 555–572.

Shirey, S.B., Klewin, K.W., Berg, J.H., Carlson, R.W., 1994. Temporal changes in the sources of flood basalts: isotopic and trace element evidence from the 1100 Ma old Keweenawan Mamainse Point formation, Ontario, Canada. Geochim. Cosmochim. Acta 58, 4475–4490.

Su, S.G., Liou, J.G., You, Z.D., Liang, F.H., Zhang, Z.M., 2005. Petrologic study of ultrahigh-pressure metamorphic cores from 100 to 2000 m depth in the main hole of the Chinese Continental Scientific Drilling project, eastern China. Int. Geol. Rev. 47, 1144–1159.

Sun, S.S., McDonough, W.F., 1989. Chemical and isotope systematics of oceanic basalts: implications for mantle composition and processes. In: Saunders, A.D., Norry, M.J. (Eds.), Magmatism in the Oceanic Basins. Geological Society, London, pp. 313–345.

Toplis, M.J., Carroll, M.R., 1995. An experimental study of the influence of oxygen fugacity on Fe–Ti oxide stability, phase relations, and mineral–melt equilibria in ferro-basaltic systems. J. Petrol. 36, 1137–1170.

Tropper, P., Manning, C.E., 2005. Very low solubility of rutile in H_2O at high pressure and temperature, and its implications for Ti mobility in subduction zones. Am. Mineral. 90, 502–505.

Van Baalen, M.R., 1993. Titanium mobility in metamorphic systems: a review. Chem. Geol. 110, 233–249.

Weiblen, P.W., Morey, G.B., 1980. A summary of the stratigraphy, petrology, and structure of the Duluth complex. Am. J. Sci. 280, 88–133.

Winter, J.D., 2001. An Introduction to Igneous and Metamorphic Petrology. Prentice-Hall Inc., p. 231.

Xu, Y., Chung, S.L., Jahn, B.M., Wu, G., 2001. Petrologic and geochemical constrains on the petrogenesis of Permian–Triassic Emeishan flood basalts in southwestern China. Lithos 58, 145–168.

Yang, H.-J., Frey, F.A., Garcia, M.O., Clague, D.A., 1994. Submarine lavas from Mauna Kea volcano, Hawaii: implications for Hawaiian shield stage processes. J. Geophys. Res. 99, 15577–15594.

Yang, H.-J., Kinzler, R.J., Grove, T.L., 1996. Experiments and models of anhydrous, basaltic olivine–plagioclase–augite saturated melts from 0.001 to 10 kbar. Contrib. Mineral. Petrol. 124, 1–18.

Yang, H.-J., Frey, F.A., Weis, D., Giret, A., Pyle, D., Michon, G., 1998. Petrogenesis of the flood basalts forming the Northern Kerguelen archipelago: implications for the Kerguelen plume. J. Petrol. 39, 711–748.

Yang, H.-J., Frey, F.A., Clague, D.A., Garcia, M.O., 1999. Mineral chemistry of submarine lavas from Hilo Ridge, Hawaii: implications for magmatic processes within Hawaiian rift zones. Contrib. Mineral. Petrol. 135, 355–372.

Zhang, R.Y., Hirajima, T., Banno, S., Cong, B., Liou, J.G., 1995. Petrology of ultrahigh-pressure rocks from the southern Su-Lu region, eastern China. J. Metamorph. Geol. 13, 659–675.

Zhang, Z.M., Xu, Z.Q., Liu, F.L., You, Z.D., Shen, Q., Yang, J.S., Li, T.F., Chen, S.Z., 2004. Geochemistry of eclogites from the main hole (100~2050 m) of the Chinese Continental Scientific Drilling Project. Acta Pet. Sin. 20, 27–42 (in Chinese with English abstract).

Zhou, M.F., Kennedy, A.K., Sun, M., Malpas, J., Lesher, C.M., 2002. Neoproterozoic arc related mafic intrusions along the northern margin of South China: implications for the accretion of Rodinia. J. Geol. 110, 611–618.